Capacitance scaling law for diatomic molecules and prediction of their electron detachment energies

James C. Ellenbogen*
Nanosystems Group, The MITRE Corporation, McLean, Virginia 22102, USA
(Received 30 March 2010; published 16 July 2010)

The variation or "scaling" of the quantum capacitances is explored for 45 diatomic molecules as a function of their dimensions. Scaling trends in the capacitances of these diatomic molecules dictate an "atoms-in-molecules" view of their valence energetics. That is, experimentally derived quantum capacitances for both homonuclear and heteronuclear diatomic molecules scale linearly with the average of the mean radii for the outermost orbitals of their component atoms. This is in accord with Maxwell's law for classical capacitors formed from two conducting atom-sized spheres in tangential contact. However, the scaling behavior for the molecules has some nonclassical features. Notably, the quantum capacitances extrapolate to *non*zero values at zero dimensions. Radius-capacitance points of the *homo*nuclear diatomics lie primarily along five scaling lines, with each determined by points for molecules composed of atoms with the same *atomic* symmetry (i.e., atoms from the same column in the periodic table). Five scaling lines for *hetero*nuclear diatomics each are determined by points for molecules of the same or similar *molecular* symmetries. The molecules' quantum capacitances are calculated from their ionization potentials (IPs) and electron affinities (EAs). Thus, equations or laws for the scaling lines impose mutual consistency conditions among these electron detachment energies for different diatomics of similar symmetries. By taking advantage of this, the linear quantum capacitance scaling laws and *ab initio* atomic mean radii are used to predict IPs for two diatomics with known EAs (Ga_2 and SeO), but for which there is no standard value of the IP. Similarly, the laws are used to predict EAs that were unknown or uncertain for several diatomics (Li_2, LiF, CSe, PN, BF, BCl, SiO, GeO, NCl, CaO, SrO, and BaO) with known IPs.

DOI: 10.1103/PhysRevA.82.012508 PACS number(s): 31.10.+z, 31.15.−p, 32.10.Hq, 31.90.+s

I. INTRODUCTION

This paper establishes a fundamental scaling equation for the quantum capacitances of diatomic molecules. Then, that equation or law is applied to calculate ionization potentials (IPs) or electron affinities (EAs) for diatomics in several cases [1] where these electron detachment energies have not been determined definitively.

For reasons that have been reviewed elsewhere [2], IPs and EAs can be difficult to measure or calculate theoretically by conventional approaches, even for the simplest of molecules, diatomics. Recently, however, a simple, alternative approach has been developed to estimate or predict EAs and IPs [3,4]. It enforces capacitance-based mutual consistency conditions between the IP and EA of a single atom or molecule, as well as among all the detachment energies for a series of atoms or molecules with similar shapes and symmetry types. In that prior work it was shown that quantum capacitances [5,6] vary or "scale" linearly with the dimensions of molecules in a sequence with similar structures. Further, it was shown that the associated simple, linear scaling relation permits the calculation of an unknown EA for a molecule in the sequence, given its dimensions and its IP, which usually are much easier to determine than the EA. Similarly, an unknown IP can be calculated if a molecule's EA is known.

Here, we demonstrate first that linear scaling principles or laws of quantum physics also apply to diatomic molecules. Specifically, in Sec. II, we show that the quantum capacitances of diatomic molecules scale linearly according to a quantum analog of Maxwell's [7,8] classical scaling law for two atom-sized spheres in tangential contact. This law shows a previously unappreciated, physics-based correlation among accepted diatomic electron detachment energies [1] determined by a number of prior investigators. Then, in Sec. III, we use that quantum capacitance scaling law to predict unknown or uncertain diatomic IPs and EAs.

II. DIATOMIC CAPACITANCE SCALING

We begin by reporting on an investigation of the scaling of the quantum capacitances for 45 diatomic molecules as a function of their atomic and molecular dimensions in cases where both the molecular IP and EA are known from experiment. As in prior work [3,4], we calculate the quantum capacitance C_σ for a neutral, many-electron quantum system σ, such as an atom X or diatomic molecule XY, using a formula due to Perdew [5] and to Iafrate *et al.* [6]:

$$C_\sigma = 1/(I_\sigma - A_\sigma). \tag{1}$$

Quantity I_σ is the valence ionization potential of a neutral system σ in its ground state and A_σ is its electron affinity (i.e., the ionization potential of its negative ion). If I_σ and A_σ are expressed in the customary units of electron volts, then Eq. (1) yields quantum capacitances in the atomic and molecular-scale units of fundamental units of positive charge per volt, which we symbolize as "$+e$/V." For homonuclear diatomic molecules ($\sigma = XX$), heteronuclear diatomic molecules ($\sigma = XY$), and atoms ($\sigma = X$ or Y), Eq. (1) is evaluated here using experimental ionization potentials and electron affinities from the online *NIST Chemistry WebBook* [1], except as noted in the tables.

*ellenbgn@mitre.org

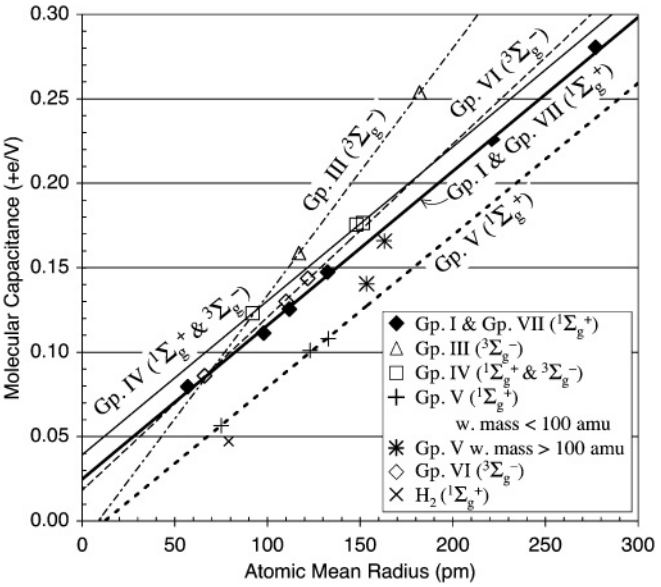

FIG. 1. Homonuclear diatomic capacitance scaling versus the mean radii of the molecules' component atoms. Quantum capacitances C_{XX} in fundamental positive charges per volt $(+e/\mathrm{V})$ for homonuclear diatomic molecules are plotted versus $\langle r\rangle_X$, the mean radii in picometers of the highest energy occupied orbitals on their component atoms. Values plotted are from Table I. In the graph, strongly linear scaling is seen for the capacitances as a function of the average of the mean atomic radii. As expressed by Eqs. (3), these trends may be interpreted in terms of a quasiclassical capacitance model in which the molecules have the structure of two conducting spheres in tangential contact. See Fig. 3(a). Collinear sets of points correspond to homonuclear diatomic molecules composed of atoms from the same column or group (Gp.) in the periodic table. Lines in the graph are determined from regression analyses, parameters for which are given in Table IIIA.

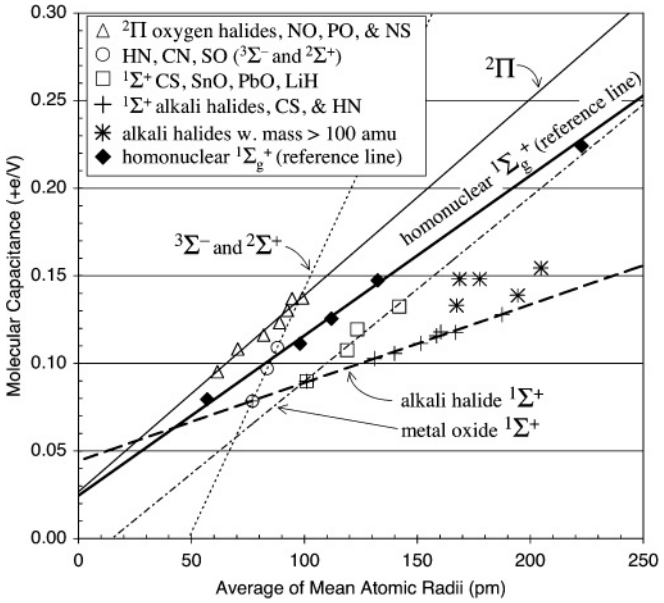

FIG. 2. Heteronuclear diatomic capacitance scaling versus the average of the mean radii of the molecules' component atoms. Quantum capacitances C_{XY} in fundamental positive charges per volt $(+e/\mathrm{V})$ for heteronuclear diatomic molecules are plotted versus $\bar{r}_{XY}$, the average of the mean radii of their component atoms in picometers. Values plotted are from Table II. Strongly linear scaling of C_{XY} with $\bar{r}_{XY}$ is seen in the graph, consistent with Eqs. (3) and supporting the two-spheres-in-contact model depicted in Fig. 3(a). Points for heteronuclear diatomics with similar molecular symmetries or term symbols λ fall on the same scaling line. Lines are determined via regression analyses, with parameters given in Table IIIB. The bold line in the graph is fit to points (black diamonds) for $^1\Sigma_g^+$ *homo*nuclear molecules from groups I and VII of the periodic table. This reference line indicates positions of heteronuclear scaling lines here relative to homonuclear scaling lines in Fig. 1.

A. Scaling law

For both homonuclear and heteronuclear diatomic molecules, it is discovered that the resulting experimentally derived quantum capacitances scale in a strongly linear manner with

$$\bar{r}_{XY} = \tfrac{1}{2}(\langle r\rangle_X + \langle r\rangle_Y). \tag{2}$$

This scaling variable is the average of the mean radii [3,9,10], $\langle r\rangle_X$ and $\langle r\rangle_Y$, for the highest occupied orbitals on a diatomic's component atoms. Of course, for homonuclear diatomics this variable reduces simply to $\langle r\rangle_X$. The linear scaling with $\bar{r}_{XY}$ is seen in the graphs in Figs. 1 and 2, which plot data from Tables I and II, respectively.

In each of the graphs, quantum capacitances C_{XY} for diatomic molecules XY that are characterized by a particular symmetry type or group λ scale along a regression line with the equation

$$C_{XY} = B_\lambda \bar{r}_{XY} + C_\lambda^{(0)} \tag{3a}$$

$$= 8\pi\epsilon_0\kappa_\lambda \ln 2\bar{r}_{XY} + C_\lambda^{(0)}. \tag{3b}$$

In Eq. (3a), the constant scaling parameters that characterize the line are B_λ, its slope, and $C_\lambda^{(0)}$, its *non*zero capacitance intercept at zero dimensions. The latter is a quantum parameter without a classical analog for an isolated capacitor [3]. Values for these scaling parameters are determined via linear regression analysis and displayed in Table III.

In Eq. (3b), the quantity $\kappa_\lambda = B_\lambda/8\pi\epsilon_0 \ln 2$ is an analog of a classical dielectric constant, but for an individual molecule XY along the scaling line λ. Values for this parameter also are given in part A of Table III.

Equation (3b) reexpresses the quantum scaling relation in a form that emphasizes its similarity to the classical scaling relation $C = 8\pi\epsilon_0\kappa \ln 2r$, which governs the capacitance for two macroscopic conducting spheres of radius r in tangential contact [7,8]. See Fig. 3(a). The quantum scaling relation, Eq. (3b), models two atomic spheres, both having the same radius $\bar{r}_{XY}$, the average of the mean radii of the two atoms.

With the exception of a few anomalous points (see Sec. II C), Eqs. (3) fit the quantum capacitance data for all the diatomics to a very high degree of confidence. This is seen in Table III, as well as in Figs. 1 and 2. In fact, as discussed in Sec. II D, this model that depends on dimensional parameters for two unbonded atoms fits the data better than other, intuitively favored diatomic capacitance models in Fig. 3 that depend upon molecular dimensional parameters describing the bound atoms.

TABLE I. Capacitances and dimensions for homonuclear diatomic molecules. Capacitances C_{XX} are reported for a number of neutral homonuclear diatomic molecules X_2 in fundamental units of positive charge per volt[a] as a function of the mean radius of the component atoms. Values of C_{XX} are calculated via Eq. (1), based upon experimental ionization potentials (I_{XX}) and electron affinities (A_{XX}) for the molecules [1], except as noted. Analogously calculated capacitances C_X for the component atoms X [3] also are included for purposes of comparison. See text. Molecules are ordered according to the group (Gp.) or column of the periodic table in which their atoms appear. See also Fig. 1.

Gp.	Molecule X_2	Mean radius[b] of atom X, $\langle r\rangle_X$ (pm)	X_2 bond length,[c] R (pm)	X_2 molecular length, $L = R + 2\langle r\rangle_X$ (pm)	X_2 equivalent radius, $r_{\rm eq} = [(\langle r\rangle_X)^2 L/2]^{1/3}$ (pm)	X_2 ionization potential,[c] I_{XX} (eV)	X_2 electron affinity,[c] A_{XX} (eV)	X_2 molecular capacitance,[d] C_{XX} ($+e$/V)	X atom capacitance,[e] C_X ($+e$/V)	Ratio $R/2\langle r\rangle_X$	Symmetry or term symbol
	H_2	79	74	232	90	15.42593	−5.78[f]	0.05	0.078	0.468	$^1\Sigma_g^+$
I	Na_2	223	308	754	266	4.892	0.430	0.22	0.218	0.690	$^1\Sigma_g^+$
I	K_2	277	391	945	331	4.062	0.497	0.28	0.260	0.705	$^1\Sigma_g^+$
VII	F_2	57	141	255	75	15.697	3.12	0.08	0.071	1.239	$^1\Sigma_g^+$
VII	Cl_2	98	199	395	124	11.48	2.5	0.11	0.107	1.014	$^1\Sigma_g^+$
VII	Br_2	112	228	452	141	10.516	2.55	0.13	0.118	1.021	$^1\Sigma_g^+$
VII	I_2	132	267	531	167	9.3074	2.524	0.15	0.135	1.007	$^1\Sigma_g^+$
III	B_2	117	159	393	139	8.1[g]	1.80	0.16	0.125	0.679	$^3\Sigma_g^-$
III	Al_2	182	247	611	216	5.4	1.46	0.25	0.180	0.677	$^3\Sigma_g^-$
IV	C_2	92	124	308	109	12.15	3.273	0.11	0.100	0.675	$^1\Sigma_g^+$
IV	Si_2	148	225	521	179	7.9	2.2	0.18	0.148	0.759	$^3\Sigma_g^-$
IV	Ge_2	152	–	–	–	7.7	2.03	0.18	0.150	–	–
V	N_2	75	110	260	90	15.5808	−2.1[h]	0.06	0.07	0.732	$^1\Sigma_g^+$
V	P_2	123	189	435	149	10.53	0.63	0.10	0.10	0.770	$^1\Sigma_g^+$
V	As_2	133	210	476	161	10.0	0.739	0.11	0.111	0.791	$^1\Sigma_g^+$
V	Sb_2	153	234	541	185	8.4	1.282	0.14	0.132	0.763	$^1\Sigma_g^+$
V	Bi_2	163	266	592	199	7.3	1.271	0.17	0.158	0.815	$^1\Sigma_g^+$
VI	O_2	66	121	253	82	12.0697	0.448	0.09	0.082	0.915	$^3\Sigma_g^-$
VI	S_2	110	189	409	135	9.356	1.670	0.13	0.121	0.859	$^3\Sigma_g^-$
VI	Se_2	122	217	460	150	8.9	1.940	0.14	0.129	0.890	$^3\Sigma_g^-$

[a]Columns marked $+e$/V report atomic and molecular capacitances in fundamental units of positive charge per volt. Multiplication by 1.602188×10^{-19} C per fundamental unit of charge converts these capacitances to the more familiar mks units of farads. Using these capacitance units gives the permittivity of free space $\epsilon_0 = 5.527350 \times 10^{-5}$ $+e$/(V pm).
[b]From Refs. [9], [10], and [13].
[c]From Ref. [1].
[d]Determined from I_{XX} and A_{XX} via Eq. (1).
[e]From Ref. [3] or via Eq. (1), using I_X and A_X from Ref. [1].
[f]A_{XX} for H_2 from Ref [14].
[g]I_{XX} for B_2 from Ref. [15].
[h]A_{XX} for N_2 from Ref. [16].

TABLE II. Capacitances and dimensions for heteronuclear diatomic molecules. Capacitances C_{XY} are reported for a number of neutral heteronuclear diatomic molecules XY in fundamental units of positive charge per volt[a] as a function of the average mean radii $\overline{r}_{XY}$ of the molecules' component atoms. Values of C_{XY} are calculated via Eq. (1), based upon experimental ionization potentials I_{XY} and electron affinities A_{XY} for the molecules [1].

Molecule XY	Mean radius[b] of atom X, $\langle r\rangle_X$ (pm)	Mean radius[b] of atom Y, $\langle r\rangle_Y$ (pm)	$\overline{r}_{XY} = (\langle r\rangle_X + \langle r\rangle_Y)/2$ (pm)	XY bond length,[c] R (pm)	Approx. molecular length, $L = R + \langle r\rangle_X + \langle r\rangle_Y$ (pm)	XY equivalent radius, $r_{eq} = [(\overline{r}_{XY})^2 L/2]^{1/3}$ (pm)	XY ionization potential,[c] I_{XY} (eV)	XY electron affinity,[c] A_{XY} (eV)	XY molecular capacitance, C_{XY} ($+e$/V)	Ratio $R/(\langle r\rangle_X + \langle r\rangle_Y)$	Symmetry or term symbol
FO	57	66	62	132	255	78	12.77	2.272	0.095	1.073	$^2\Pi$
ClO	98	66	82	172	336	104	10.885	2.2775	0.116	1.047	$^2\Pi_{3/2}$
BrO	112	66	89	157	335	110	10.46	2.353	0.123	0.882	$^2\Pi_{3/2}$
IO	132	66	99	187	385	124	9.66	2.378	0.137	0.941	$^2\Pi_{3/2}$
NO	75	66	71	115	256	86	9.2642	0.026	0.108	0.816	$^2\Pi_r$
PO	123	66	95	148	337	115	8.39	1.092	0.137	0.781	$^2\Pi_r$
NS	75	110	93	149	334	113	8.87	1.194	0.130	0.808	$^2\Pi_r$
HN	79	75	77	104	258	91	13.1	0.370	0.079	0.673	$^3\Sigma^-$
CN	92	75	84	117	284	100	14.17	3.862	0.097	0.702	$^2\Sigma^+$
SO	110	66	88	148	324	108	10.294	1.125	0.109	0.842	$^3\Sigma^-$
LiH	205	79	142	159	443	165	7.9	0.342	0.132	0.562	$^1\Sigma^+$
SnO	172	66	119	183	421	144	9.9	0.598	0.108	0.770	$^1\Sigma^+$
PbO	181	66	123	192	439	150	9.1	0.722	0.119	0.778	$^1\Sigma^+$
CS	92	110	101	153	355	122	11.33	0.205	0.090	0.760	$^1\Sigma^+$
NaF	223	57	140	193	472	167	9.98	0.52	0.106	0.689	$^1\Sigma^+$
KF	277	57	167	217	551	197	9.54	1.04	0.118	0.650	$^1\Sigma^+$
LiCl	205	98	152	202	505	180	9.57	0.593	0.111	0.667	$^1\Sigma^+$
NaCl	223	98	160	236	557	193	9.2	0.727	0.118	0.736	$^1\Sigma^+$
KCl	277	98	188	267	642	224	8.4	0.582	0.128	0.711	$^1\Sigma^+$
LiBr	205	112	158	217	534	188	9.3	0.660	0.116	0.685	$^1\Sigma^+$
NaBr	223	112	167	250	585	201	8.3	0.788	0.133	0.748	$^1\Sigma^+$
KBr	277	112	194	282	671	233	7.85	0.642	0.139	0.726	$^1\Sigma^+$
LiI	205	132	169	239	577	202	7.5	0.750	0.148	0.709	$^1\Sigma^+$
NaI	223	132	178	271	626	215	7.62	0.87	0.148	0.764	$^1\Sigma^+$
KI	277	132	205	305	714	246	7.2	0.728	0.155	0.744	$^1\Sigma^+$

[a]See footnote a of Table I.
[b]From Refs. [9], [10], and [13].
[c]From Ref. [1].

TABLE III. Regression parameters and dielectric constants. Parameters determined by linear regression from fits of diatomic quantum capacitances to $\bar{r}_{XY}$ via Eqs. (3). Parameters in part A describe homonuclear capacitances from Table I that scale along five different regression lines, according to the column or group (Gp.) in the periodic table of the molecules' atoms. Part B describes heteronuclear capacitances from Table II that scale along four different lines, according to the symmetry of the molecules' ground neutral states. See Figs. 1 and 2, as well as Secs. II A and II B.

Group or symmetry, λ	Slope, B_λ [$+e$/(V pm)]	Intercept, $C_\lambda^{(0)}$ ($+e$/V)	Dielectric constant,[a] κ_λ	Goodness of fit, R^2
A. Homonuclear scaling parameters				
I and VII ($^1\Sigma_g^+$)	9.12×10^{-4}	0.0247	0.947[b]	0.998
III ($^3\Sigma_g^-$)	1.46×10^{-3}	0.0124	1.520[b]	1
IV ($^1\Sigma_g^+$&$^3\Sigma_g^-$)	9.12×10^{-4}	0.0392	0.947[b]	0.998
V ($^1\Sigma_g^+$)	9.00×10^{-4}	−0.0108	0.935[b]	0.999
VI ($^1\Sigma_g^+$)	1.03×10^{-3}	0.0182	1.066[b]	0.999
B. Heteronuclear scaling parameters				
$^1\Sigma^+$ (a.h.)[c]	4.47×10^{-4}	0.0443	0.464[b]	0.996
$^1\Sigma^+$ (ox.)[d]	1.05×10^{-3}	−0.0155	1.091[b]	0.967
$^3\Sigma^-$ and $^2\Sigma^-$	2.78×10^{-3}	−0.135	2.888[b]	1.000
$^2\Pi$	1.12×10^{-3}	0.0267	1.163[b]	0.971

[a]Assumes value $\epsilon_0 = 5.526\,349 \times 10^{-5}$ $+e$/(V pm) for permittivity of free space.
[b]For two-spheres-in-contact model, $\kappa_\lambda = B_\lambda / 8\pi\epsilon_0 \ln 2$.
[c]a.h. $= {}^1\Sigma^+$ diatomics that scale like alkali-metal halides, per Sec. II B.
[d]ox. $= {}^1\Sigma^+$ diatomics that scale like metal oxides, per Sec. II B.

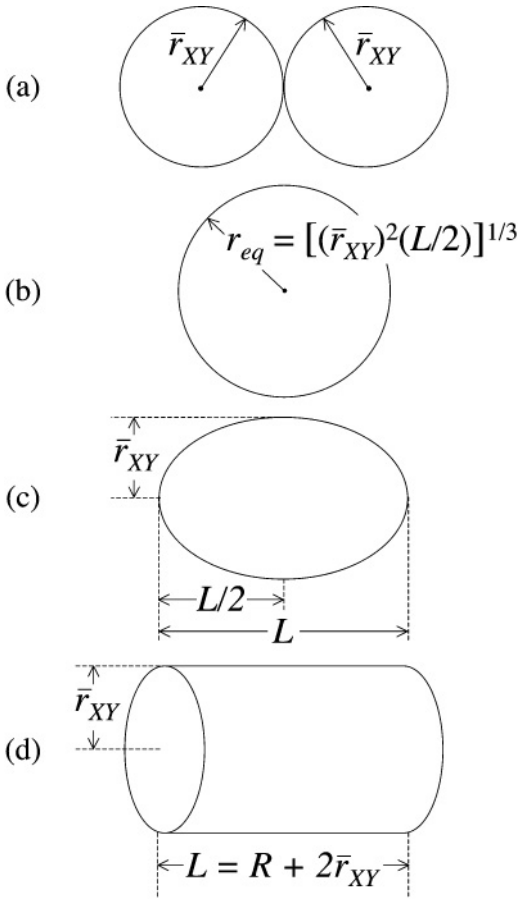

FIG. 3. Four classical capacitance models for diatomic molecular capacitors. These are (a) two spheres in tangential contact, (b) an isoperimetric sphere, (c) an ellipsoid of revolution, and (d) a truncated cylinder. Computational experiments in this work show that model (a) best fits the diatomic molecule quantum capacitance scaling data from prior experiments and *ab initio* calculations. See Figs. 1 and 2, Sec. II D, and Table III. However, classical models (a), (b), and (d) all account reasonably well for the quantum data. Model (b) approximates model (c), because the capacitance of an isoperimetric sphere [4] is predicted [11,12] and also found by direct calculation to be a tight lower bound to that of an ellipsoid of revolution with the dimensions of the diatomic molecules. Another model discussed in the text, scaling simply with molecular length L, is not depicted here.

B. Key features of scaling behavior

In Fig. 1, radius-capacitance points for *homo*nuclear diatomics are seen to segregate themselves primarily into five collinear sets. Each of these sets contains points that represent molecules composed of atoms with the same *atomic* angular momentum symmetry [i.e., atoms from the same "group" (Gp.) or column λ in the periodic table]. Homonuclear diatomics composed of atoms from one group have points that fall on a different line than homonuclear diatomics composed of atoms from another group in the periodic table (except that points for groups I and VII fall on the same line). Lines in the figure are determined via linear regression analyses that were performed separately on each of these five sets of points. The resulting regression parameters for the homonuclear diatomics are presented in part A of Table III.

In contrast to the homonuclear case, in Fig. 2 points for the *hetero*nuclear diatomics are seen to segregate themselves into collinear sets according to the angular momentum symmetries or term symbols λ for the ground neutral states of the *molecules*. There are four such sets for the heteronuclear diatomics shown in the graph in Fig. 2, with the corresponding lines in the graph determined via linear regression and the regression parameters reported in part B of Table III.

It is primarily the case that each different heteronuclear diatomic capacitance scaling line is associated with a different symmetry type and vice versa. An exception is that the heteronuclear diatomics of $^1\Sigma^+$ symmetry have points that are segregated into at least two different collinear groups. In Fig. 2, one group of points (+ symbols) for the $^1\Sigma^+$ diatomics includes those for most of the alkali-metal halide (a.h.) molecules, as well as CS and HN; the other group includes points (□ symbols) for the metal oxides PbO and SnO (ox.), as well as for CS and LiH.

Additionally, as noted in Table IV and Sec. III D, the alkaline earth metal monoxides BeO and MgO may constitute yet a third uniquely scaling group of $^1\Sigma^+$ heteronuclear diatomics with a fifth heteronuclear scaling line. The radius-capacitance points for these molecules are not displayed in the graph in Fig. 2, though, because their capacitance coordinates are known with less confidence. They are based on EAs from theory that are not listed in the *NIST Chemistry WebBook* [1].

Observe in Fig. 2 that the point for the CS molecule is taken to be a member of both the alkali-metal halide and the metal oxide $^1\Sigma^+$ groups; the CS point lies at the intersection of the lines defined by each. Similarly, the HN point at the intersection of the alkali-metal halide $^1\Sigma^+$ scaling line and the scaling line for $^3\Sigma^-$ and $^2\Sigma^+$ molecules is taken to be a member of both groups. (Those intersection points are represented on the graph by both a cross and a square or circle that overlaps it.)

More generally, in both Fig. 1 and Fig. 2 it is seen that there is a radius-capacitance point at or near almost every intersection of two scaling lines. For example, in Fig. 1 the O_2 point is at the intersection of three lines (the Gp. III, Gp. VI, and the Gp. I and VII lines), while the C_2 point is at the intersection of the Gp. III and Gp. IV lines. In Fig. 2, beyond the intersections visible in the graph that occur at or near heteronuclear radius-capacitance points, the metal oxide $^1\Sigma^+$ line intersects the $^1\Sigma_g^+$ *homo*nuclear scaling line at a point off the graph to the right that nearly coincides with the radius-capacitance point for the molecule K_2 on the bold black reference line.

It is notable in Fig. 2, as well, that this reference homonuclear scaling line has very nearly the same nonzero intercept with the vertical axis as the line for $^2\Pi$ heteronuclear molecules. Further, we see in Fig. 1 that three of the capacitance scaling lines for the homonuclear diatomics are nearly parallel. These are the lines associated with atoms in groups I and VII, Gp. IV, and Gp. V. Such coincident intersections, intercepts, and slopes in the plots of C_{XY} versus $\bar{r}_{XY}$ suggest a discreteness in the values of the quantum capacitances and atomic radii.

This discreteness and most of the other qualitative features described in this section for diatomic capacitance scaling with respect to $\bar{r}_{XY}$ also persist when scaling is considered relative to other dimensional scaling variables for diatomics. See Fig. 3 and Sec. II D.

C. Scaling anomalies

Despite very strong linear fits of C to $\bar{r}_{XY}$ for most of the diatomic molecules, as just summarized, there are some notable exceptions. The large IP, negative EA, and consequent small capacitance for H_2 places its point ($\times$) below all the homonuclear scaling lines in Fig. 1. Physically, this probably is because of the H_2 molecule's small number of electrons and the similarity of its electron configuration to that of the He atom. This makes the H_2 electron distribution resistant to polarization and limits its ability to store positive charge relative to its size.

However, the opposite tendency is observed in the radius-capacitance points for two larger sets of exceptions to linear capacitance scaling with $\bar{r}_{XY}$. These exceptions have anomalously large capacitances for their size and are represented by the large asterisks ($*$ symbols) in Figs. 1 and 2. In both the homonuclear plot and heteronuclear plot, these anomalous points represent a few heavier diatomics that (a) have total nuclear masses greater than 100 amu and (b) also have the same symmetry type as lighter molecules that fall along the scaling line with the lowest overall capacitances. In the homonuclear case this corresponds to the heavier Gp. V diatomic molecules and in the heteronuclear case it corresponds to the heavier alkali-metal halide diatomics. These anomalies persist when the capacitances are plotted versus other diatomic dimensional variables, such as are described in Fig. 3 and in Sec. II D.

Empirically, these anomalies arise because of unusually small IPs and large EAs for the heavy molecules, leading to unusually large capacitances relative to the molecules' sizes or the radii of their component atoms. In the case of the Gp. V homonuclear diatomic molecules, the source of anomalies in Fig. 1 for Sb_2 and Bi_2 appears to be that component atoms, Sb and Bi, also have anomalously large capacitances. Mean radius-capacitance points for those heavy atoms likewise lie above a scaling line for lighter Gp. V atoms [17].

A similar explanation does not seem to account for anomalies in Fig. 2 in the case of the alkali-metal halides, however. Atomic capacitances of Br and I would scale right on a mean radius-capacitance line determined by lighter atoms F and Cl. Also, capacitances for Li, Na, and K scale on a line [3]. We have not yet found a satisfactory explanation for the anomalies in the heteronuclear case.

D. Comparisons with alternative capacitance models

As indicated in Sec. II A, for the preponderance of nonanomalous diatomic quantum capacitance points it was found that the two-spheres-in-contact model of Eqs. (3) and Fig. 3(a) provided the best fit to the diatomic quantum capacitances as a function of atomic or molecular dimensions. This was determined by comparing the goodness of fit for Eq. (3a) with fits for regression equations associated with several other quasiclassical capacitance models.

These other models included linear scaling with the molecules' isoperimetric equivalent radii [4,11,12]

$$r_{\mathrm{eq}} = [(\bar{r}_{XY})^2 L/2]^{1/3}, \tag{4}$$

as depicted schematically in Fig. 3(b). For this model, we also verified numerically that the quantity $4\pi\epsilon_0 r_{\mathrm{eq}}$ is a close lower bound [11] to the capacitances of ellipsoids [4] that have the dimensions of the molecules. [See Fig. 3(c).] Thus, exploration of the scaling with r_{eq} also served to explore how well a proposed [18] ellipsoidal capacitor model represents the behavior of the quantum capacitances of the diatomics.

Another model that was tried represented the diatomic capacitors as truncated cylinders [8], as in Fig. 3(d). Finally, the alternative models included one in which the capacitances scale simply with the approximate molecular lengths,

$$\begin{aligned} L &= R + \langle r \rangle_X + \langle r \rangle_Y \\ &= R + 2\bar{r}_{XY}, \end{aligned} \tag{5}$$

where R is the equilibrium bond length.

All the regression models produced graphs similar in general appearance to Figs. 1 and 2. For example, all yielded five homonuclear and four heteronuclear scaling lines, as well as other of the key qualitative features discussed in Secs. II B and II C.

However, compared with these others, the two-spheres-in-contact model gives the highest overall values of the correlation coefficients (R^2) for the fits to the five homonuclear and four heteronuclear scaling lines. Especially, as seen in Table III,

this preferred model did not have any values of R^2 that are much lower than approximately 0.97, as all the others did.

For example, consider the best of the alternative models, the isoperimetric sphere or the nearly equivalent ellipsoid of revolution capacitance model. For fits to capacitances arising from all five groups of homonuclear diatomics, as well as from three of the groups of heteronuclear diatomics, the regression formula for the isoperimetric model yielded nearly the same high R^2 values as listed in Table III for the two-spheres-in-contact model. However, in the case of the $^2\Pi$ heteronuclear diatomics, the isoperimetric sphere model was appreciably worse, giving a correlation coefficient of only 0.934. The other alternative capacitance models also worked well for the homonuclear data, but they did not work well in the case of one or more of the groups of heteronuclear systems.

A similar limitation is exhibited by a variant of the two-spheres-in-contact model that uses as the dimensional variable another isoperimetric [11,12] measure, the square root of the sum of the surface areas of the two atomic spheres. This explicitly represents the effect of unequal mean radii of atoms in heteronuclear diatomics. As with the other alternative models, this model works well for all the homonuclear molecules, plus two groups of heteronuclear systems. However, it does not fit the $^2\Pi$ capacitances quite as well as a fit to $\bar{r}_{XY}$ and it breaks down for the molecules with atoms most disparate in radius, the alkali-metal halide $^1\Sigma^+$ molecules, giving a fit with only $R^2 = 0.944$. [See Sec. II E for a rationale why Eqs. (3) continue to work well for the alkali-metal halides.]

So that the reader easily can verify these comparisons, values of the alternative dimensional scaling variables are given in Tables I and II. Based on such comparisons, the two-spheres-in-contact model of Eqs. (3) is judged to be the best physical representation of the diatomic capacitors.

This quasiclassical capacitance model is a kind of "atoms-in-molecules" model in that it expresses the molecular quantum capacitances solely in terms of the mean dimensions of the component atoms. These have been rigorously determined to high accuracy in *ab initio* quantum calculations [9,10,13]. This is a significant advantage in that it eliminates any need to know the dimensions of the entire molecule, which are much more difficult to define or determine in a rigorous manner.

E. Rationale for the two-spheres-in-contact model

An after-the-fact rationale for the success of the two-spheres-in-contact model can be derived via a visual comparison of homonuclear diatomic capacitances C_{XX} with values for capacitances C_X of their component atoms. (See columns 9 and 10 of Table I.) This comparison reveals that for most of the homonuclear diatomics $C_{XX} \approx C_X$. Linear regression analysis of (C_X, C_{XX}) points, excluding outliers for H_2 and Al_2, confirms this observation: $C_{XX} = 1.101 C_X + 0.002$, with a correlation coefficient of $R^2 = 0.963$. Based on these observations, one might say that it is no surprise that C_{XX} should scale linearly with $\langle r \rangle_X$ in the homonuclear case, because we have shown previously [3] that C_X does. By this *a posteriori* reasoning, one might see the strong linear correlation of C_{XY} with $\bar{r}_{XY}$ in the heteronuclear case simply as a consequence of the fact that this dimensional parameter creates an underlying *homo*nuclear-type two-spheres-in-contact capacitance model for the *hetero*nuclear species, involving two model pseudoatoms of equal radius $\bar{r}_{XY}$.

The initial hypothesis of this work was, however, that the molecular capacitance scaling would depend most strongly on molecular dimensions. Much investment of effort was made in testing models with that feature. The now-preferred two-spheres-in-contact model was tested as a last option. The author still sees as remarkable the consequence of this model having proven so accurate in representing the capacitances of diatomic molecules in terms of their atoms' mean radii. The consequence is that such fundamentally molecular properties of diatomics as their electron detachment energies also appear to be dependent on purely atomic dimensional parameters. This consequence is applied in the next section.

III. PREDICTIONS

In this section, it is demonstrated that the quantum capacitance scaling trends observed in Sec. II for diatomic molecules with known electron detachment energies can be applied to predict or estimate unknown or uncertain diatomic electron detachment energies with reasonable accuracy. It also is shown that these trends can be used to assess the consistency of individual IP or EA values with other detachment energies determined for the same or related diatomic species.

Predictions of previously unknown or uncertain diatomic IPs and EAs are given in Table IV. The equations and steps for making these predictions are detailed in the next two sections. A critical analysis of these predictions is given in Sec. III C.

A. Diatomic ionization potentials

For the diatomics Ga_2 and SeO, the *NIST Chemistry WebBook* [1] does not list an IP. In each case we are able to use the capacitance scaling laws to predict the IP via the following approach. Equation (1), with $\sigma = XY$, may be solved for I_{XY} in terms of A_{XY} and C_{XY}. Then, the strong linear fit of C_{XY} to $\bar{r}_{XY}$ for the homonuclear and heteronuclear diatomics permits us to eliminate C_{XY} in favor of the right-hand side of the regression equation (3a), as follows:

$$I_{XY} = A_{XY} + \frac{1}{C_{XY}} \tag{6a}$$

$$= A_{XY} + \frac{1}{B_\lambda \bar{r}_{XY} + C_\lambda^{(0)}}. \tag{6b}$$

By using Eq. (6b), it becomes a simple matter to predict the IPs of diatomic molecules, such as Ga_2 and SeO, for which the capacitance scaling parameters and the EAs are known.

For example, since Ga_2 is composed of atoms from Gp. III of the periodic table, we take the corresponding values from Table IIIA for the scaling parameters B_λ and $C_\lambda^{(0)}$, along with the *NIST Chemistry WebBook* value of $A_{GaGa} = 1.60$ eV, which also is reported in the second line of column 10 in Table IV. Substituting these values in Eq. (6b), one obtains $I_{GaGa} = 5.56$ eV, as listed in the second line of column 9 in Table IV.

Similarly, since the symmetry of heteronuclear SeO is $\lambda = {}^3\Sigma^-$, one uses in Eq. (6b) the scaling parameters for the $^3\Sigma^-$ and $^2\Sigma^-$ molecules from Table IIIB, along with the value

of A_{XY} listed for SeO in column 10 of Table IV. The value obtained, as listed in column 9 of Table IV, is $I_{\mathrm{SeO}} = 9.4$ eV.

B. Diatomic electron affinities

A number of diatomics listed in the *NIST Chemistry WebBook* [1] have IPs tabulated for them, but no EAs. To use capacitance scaling to make predictions of these previously unknown or uncertain diatomic EAs, we derive analogs of Eqs. (6) that evaluate A_{XY} based upon capacitance scaling:

$$A_{XY} = I_{XY} - \frac{1}{C_{XY}} \tag{7a}$$

$$= I_{XY} - \frac{1}{B_\lambda \bar{r}_{XY} + C_\lambda^{(0)}}. \tag{7b}$$

As in the case of Eqs. (6), these equations follow from Eqs. (1) and (3a).

In a fashion similar to the IP calculations just described, Eq. (7b) is evaluated to predict values of A_{XY}, using data from Tables III and IV. Such calculations are performed here for the homonuclear diatomic molecule Li_2 and the heteronuclear diatomics LiF, CSe, PN, BF, BCl, SiO, GeO, NCl, CaO, SrO, and BaO. The predicted values of their EAs are listed in column 11 of Table IV.

However, for several of the heteronuclear diatomics of $^1\Sigma^+$ symmetry there is ambiguity as to which of the two scaling lines for that symmetry their capacitance scaling points should lie upon. For this reason, we calculate and list in Table IV the EAs that would arise from both choices. However, in the footnotes to the table and in Sec. III C we attempt to resolve some of these ambiguities. Also, for a few of the molecules of interest, there is more than one plausible choice for the IP [1]. In those cases, we used Eq. (7b) to predict the EAs that would arise for all those plausible choices. All these results for A_{XY} are given in column 11 of Table IV.

In cases such as BF where the capacitance-based method predicts a negative EA, no matter which scaling line is chosen, we believe this indicates that the extra electron on the anion is unbound (or only very weakly bound). We have no evidence, though, that the absolute magnitudes of our negative EA predictions are accurate.

C. Comparison of predictions here with results from other sources

For consistency and to ensure that our major results are based upon the most widely accepted and widely available data, we have employed in our analysis to this point electron detachment energies obtained almost exclusively from the online *NIST Chemistry WebBook* [1]. However, for thoroughness and as an important cross-check, in Table V and in this section we compare our predictions of diatomic electron detachment energies in the upper portion of Table IV with theoretical predictions and experimental measurements that have been compiled in two additional authoritative, though less widely available compendiums: (a) a 2002 review by Schaefer and his collaborators [21] of molecular electron affinities from experiment and theory and (b) the 1997 *Diatomix Database* of IPs, EAs, and other data about diatomic molecules compiled by Simons and his collaborators [19].

In the first three lines of Table V is seen a comparison of our ionization potential predictions for Ga_2 and SeO, as well as our electron affinity prediction for the diatomic molecule Li_2, with values given in the two compendiums just cited. Both of our IP predictions are seen to be in reasonably good agreement with the experimentally derived values. Likewise, our EA prediction for Li_2 is seen to be in reasonable agreement with the theoretical and experimental values from the alternative sources. This agreement is particularly notable given how little computational work is necessary to obtain our predictions, compared with the much greater effort required to obtain the comparable values listed in the other sources.

It also is seen in the last two lines of Table V that our prediction of the EA of SiO using the $^1\Sigma^+$ alkali-metal-halide-type (a.h.) capacitance scaling parameters falls within the range of other theoretical predictions of this quantity, which vary considerably. In contrast, our prediction using the $^1\Sigma^+$ metal oxide-type (ox.) scaling does not fall in the range of those other predictions. This suggests that the quantum capacitance of the $^1\Sigma^+$ neutral SiO molecule scales on the line with the alkali-metal halide diatomics, not on the scaling line with the metal oxides. This "preferred" alkali-metal halide scaling is indicated via note d in Table IV. It is not clear yet, though, how one would discern this counterintuitive preferred scaling *a priori*, with high confidence. Thus, our effort at prediction for SiO itself is only partially successful.

However, the fact that SiO probably scales on the alkali-metal halide scaling line suggests strongly that GeO does, as well (since Ge is immediately below Si in the same column of the periodic table). Thus, the additional theoretical guidance in selecting the scaling line for SiO enables us to select a preferred scaling for GeO, also, and thereby assert, from the two GeO results in Table IV, that the electron affinity of GeO is $A_{\mathrm{GeO}} = 0.35$ eV. This is a quantity for which there is no prior theoretical or experimental value listed in the major authoritative reference works [1,19,21,29].

For PN, the lack of agreement with experiment seen in Table V for our EA predictions from Table IV seems, at first, to rule out both the alkali-metal-halide-type scaling and the metal-oxide-type scaling. (See the first two lines listed for PN in Table V.) However, in the third and fourth lines listed for PN in Table V we see that predictions within the error bounds of the experiment result for both scalings if a smaller, adiabatic value [19,27] of I_{XY} is used to calculate A_{XY} via Eq. (7b).

Finally, in the fourth line of Table V, it is troubling that our capacitance-based prediction of 1.58 eV for the EA of LiF is so far from agreement with a theoretical result of 0.36 eV due to Gutsev *et al.* [20] that is judged elsewhere [19] to be accurate. The discrepancy of approximately 1.2 eV with our calculation via Eq. (7b) could not be reconciled by taking into account the small variations in the values given for the LiF IP, as determined by different methods and listed in different sources [1,19]. On the other hand, our prediction of the EA for LiF is consistent with the lower bound of 1.35 eV for the EA that appears online in the *NIST WebBook* [1,30]. Additionally, the scaling trend upon which we base our prediction arises from a fit with high confidence ($R^2 = 0.996$) to points representing many of the lighter alkali-metal halide

TABLE IV. Predictions of ionization potentials, I_{XY}, and electron affinities, A_{XY}, for diatomic molecules XY. Values of I_{XY} and A_{XY} are predicted for diatomic molecules for which there presently are no accepted values in the tables in the authoritative online *NIST Chemistry WebBook* [1] or for which there are several different contending values. Equations (6b) and (7b) are used to predict the IPs and EAs, respectively. See Sec. III for details. In the upper portion of the table, in several cases it is not clear upon which of two scaling lines a molecule of $^1\Sigma^+$ symmetry should be placed. In such cases, we report two possible predictions of A_{XY} for a diatomic molecule with $^1\Sigma^+$ symmetry, depending upon whether its radius-capacitance point is placed upon the scaling line in Fig. 2 for the alkali-metal halides (a.h. scaling line) or the one for SnO and PbO (oxide scaling line). In some of these cases, there is evidence that might resolve these ambiguities, as indicated by notes a and d. Additionally, if two plausible values of I_{XY} are reported for a molecule in the *NIST WebBook*, this leads via Eq. (7b) to two different values of A_{XY}. Both possibilities are reported in separate lines, as indicated by note c.

Molecule XY	Term symbol or symmetry type and scaling line	Capacitance scaling parameters B_λ [$+e$/(V pm)]	Capacitance scaling parameters $C_\lambda^{(0)}$ ($+e$/V)	Mean radius of atom X, $\langle r\rangle_X$ (pm)	Mean radius of atom Y, $\langle r\rangle_Y$ (pm)	Average mean radii, of atoms $\bar{r}_{XY} = (\langle r\rangle_X + \langle r\rangle_Y)/2$ (pm)	I_{XY} Accepted value [1] (eV)	I_{XY} Prediction of this work (eV)	A_{XY} Accepted value [1] (eV)	A_{XY} Prediction of this work (eV)	Notes
Predictions based on scaling parameters and detachment energies from *NIST Webbook* [1]. See Secs. III A and III B.											
Li_2	$^1\Sigma_g^+$	9.12×10^{-4}	0.0247	205	205	205	5.1127		none	0.39	
Ga_2	$^3\Sigma_g^-$	1.46×10^{-3}	−0.0124	181	181	181	none	5.56	1.60		
LiF	$^1\Sigma^+$ (a.h. scaling)	4.47×10^{-4}	0.0443	205	57	131	11.3		>1.35	1.58	
CSe	$^1\Sigma^+$ (a.h. scaling)	4.47×10^{-4}	0.0443	92	122	107	10.94		none	0.088	
	$^1\Sigma^+$ (oxide scaling)	1.05×10^{-3}	−0.0154	92	122	107	10.94		none	0.65	a
PN	$^1\Sigma^+$ (a.h. scaling)	4.47×10^{-4}	0.0443	123	75	99	11.88		none	0.59	b
PN	$^1\Sigma^+$ (oxide scaling)	1.05×10^{-3}	−0.0154	123	75	99	11.88		none	0.61	b
BF	$^1\Sigma^+$ (a.h. scaling)	4.47×10^{-4}	0.0443	117	57	87	11.12		none	−0.90	
	$^1\Sigma^+$(oxide scaling)	1.05×10^{-3}	−0.0154	117	57	87	11.12		none	−2.02	
BCl	$^1\Sigma^+$ (a.h. scaling)	4.47×10^{-4}	0.0443	117	98	108	10.2		none	−0.63	
	$^1\Sigma^+$ (oxide scaling)	1.05×10^{-3}	−0.0154	117	98	108	10.2		none	−0.035	
BCl	$^1\Sigma^+$ (a.h. scaling)	4.47×10^{-4}	0.0443	117	98	108	12		none	1.18	c
	$^1\Sigma^+$ (oxide scaling)	1.05×10^{-3}	−0.0154	117	98	108	12		none	1.77	c
SiO	$^1\Sigma^+$ (a.h. scaling)	4.47×10^{-4}	0.0443	148	66	107	11.49		none	0.64	d
SiO	$^1\Sigma^+$ (oxide scaling)	1.05×10^{-3}	−0.0154	148	66	107	11.49		none	1.20	
GeO	$^1\Sigma^+$ (a.h. scaling)	4.47×10^{-4}	0.0443	152	66	109	11.1		none	0.35	d
GeO	$^1\Sigma^+$ (oxide scaling)	1.05×10^{-3}	−0.0154	152	66	109	11.1		none	1.03	
SeO	$^3\Sigma_{0+}^-$	2.78×10^{-3}	−0.1352	122	66	94	none	9.4	1.456		
NCl	$^3\Sigma^-$	2.78×10^{-3}	−0.1352	75	98	87	9.69		none	0.17	
Predictions and scaling parameters based, in part, on electron affinities from alternative sources [19,20]. See Sec. III D.											
BeO	$^1\Sigma^+$	2.84×10^{-3}	−0.1668	140	66	103	10.1		2.15		e
MgO	$^1\Sigma^+$	2.84×10^{-3}	−0.1668	172	66	119	7.4		1.56		e
CaO	$^1\Sigma^+$	2.84×10^{-3}	−0.1668	223	66	145	6.66		none	2.56	f
SrO	$^1\Sigma^+$	2.84×10^{-3}	−0.1668	245	66	156	6.6		none	2.96	f
BaO	$^1\Sigma^+$	2.84×10^{-3}	−0.1668	278	66	172	6.46		none	3.35	f

[a]Preferred prediction for A_{XY} because value should be greater than that for CS, since CSe has atoms from the same columns of the periodic table but is larger in size. Prediction from the other $^1\Sigma^+$ scaling line yields value of A_{XY} smaller than that for CS.

[b]Unable to discriminate which $^1\Sigma^+$ scaling line PN radius-capacitance point should lie on. However, both scaling lines give approximately the same prediction, $A_{XY} \approx 0.6$ eV.

[c]Employed alternative value of I_{XY} from Ref. [1] in this line to predict A_{XY}.

[d]Preferred scaling and prediction. See rationale in Sec. III C.

[e]I_{XY} from Ref. [1] and A_{XY} from Ref. [20] used to determine scaling parameters B_λ and $C_\lambda^{(0)}$.

[f]I_{XY} from Ref. [1] and LiO-MgO scaling parameters used to predict A_{XY}.

TABLE V. Comparison of electron detachment energies predicted in this work with theoretical and experimental values compiled in the *Diatomix Database* [19] and by Rienstra-Kiracofe *et al.* [21]. For diatomics having alternative values listed in these compilations, those are compared to values predicted in this work and listed in Table IV. In other cases, no authoritative alternative values are readily available.

Diatomic XY	Scaling line	This work	Other theory	Experiment
		Ionization potentials, I_{XY}, in eV		
Ga_2	Gp. III($^3\Sigma_g^-$)	5.56		5.9 ± 0.2[a]
SeO	$^3\Sigma^-$	9.4		9.9 ± 0.3[b]
		Electron affinities, A_{XY}, in eV		
Li_2	Gp. I($^1\Sigma_g^+$)	0.39	0.431[c]	0.437 ± 0.009[d]
LiF	$^1\Sigma^+$(a.h)	1.58	0.36[e]	
PN	$^1\Sigma^+$(a.h.)	0.59		0.32 ± 0.20[f]
	$^1\Sigma^+$(ox.)	0.61		
	$^1\Sigma^+$(a.h.)	0.12[g]		
	$^1\Sigma^+$(ox.)	0.14[g]		
SiO	$^1\Sigma^+$(a.h.)	0.64	0.11−0.75[h]	
	$^1\Sigma^+$(ox.)	1.20		

[a]Experimental value from Refs. [19,22].
[b]Experimental value from Refs. [19,23].
[c]Other theory result from Refs. [19,24].
[d]Experimental value from Refs. [21,25].
[e]Other theory result from Refs. [19,20].
[f]Experimental value from Refs. [19,26].
[g]Alternative prediction uses adiabatic IP = 11.41 eV from Refs. [19, 27]; yields EA result within error bounds of experiment.
[h]Other theory results from Refs. [21,28].

molecules, as seen in Fig. 2. Thus, this scaling line should provide a strong mutual consistency condition for the IPs and EAs of all the light alkali-metal halide molecules. By those standards, Gutsev's value of 0.36 eV for the EA of LiF seems to be too low. It is inconsistent with the generally accepted values for its IP and with the electron detachment energies of the other light alkali-metal halide diatomics. This inconsistency suggests that further experimental or theoretical effort to verify the EA (and, possibly, the IP) of LiF might be in order.

D. Further predictions of electron detachment energies based on data from other sources

By taking advantage of electron affinity values listed in the supplemental sources described in the last section, we also were able to determine provisionally, from only two theory points, an additional, fifth quantum capacitance scaling line for the heteronuclear diatomics. The line describes scaling of the capacitances for the $^1\Sigma^+$ alkaline earth metal monoxide diatomics BeO, MgO, CaO, SrO, and BaO. Parameters for this scaling line were evaluated using the known IPs and EAs of just the two lightest molecules in this sequence, BeO and MgO. (See the fourth and fifth lines from the bottom of Table IV.) The BeO and MgO IPs there were taken from the *NIST Chemistry WebBook* [1], but the EAs for these two species, as calculated in earlier theoretical work [20], were obtained from the *Diatomix Database* [19].

Then, we used in Eq. (7b) the scaling parameters and the known [1] IPs for the heaviest three molecules in this sequence, CaO, SrO, and BaO. Thereby, in the last three lines of Table IV we predict the otherwise unknown EAs for CaO, SrO, and BaO. Values for their EAs do not seem to be available elsewhere in the literature [1,19,21,29].

IV. SUMMARY AND CONCLUSIONS

In this paper, we have used diatomic ionization potentials and electron affinities from standard tables [1], along with atomic mean radii from *ab initio* calculations [9,10,13], to extend to diatomic molecules recent demonstrations that atoms and molecules behave much like classical capacitors. As has been shown for atoms [3] and organic molecules [4], quantum capacitances of diatomic molecules vary linearly with the tiny systems' dimensions, much like the classical capacitances of macroscopic conductors. For diatomics, this quasiclassical behavior was shown to conform with Eqs. (3).

From Eqs. (3), diatomic molecular properties that usually are thought to depend upon the character and dimensions of the bonded assembly of atoms, appear to depend simply on the dimensions of the unbonded atoms. The capacitance model of Eqs. (3) treats the diatomic molecule as two unperturbed atom-sized spheres in tangential contact. For 45 diatomic molecules, this empirically dictated "atoms-in-molecules" type model proves highly accurate and better than intuitively favored models with more explicit dependence on molecular dimensional parameters, such as the bond length.

The linear equations or laws of quantum capacitance scaling associated with this model imply mutual consistency conditions, Eqs. (6) and (7), among the ionization potentials and electron affinities for diatomic molecules of similar symmetries. Equations (6) have been used here to predict IPs for two diatomics with known EAs (Ga_2 and SeO) but for which there is no standard value of the IP. Similarly, Eqs. (7) have been used to estimate or predict EAs that are unknown or uncertain for several diatomics with known IPs (Li_2, LiF, CSe, PN, BF, BCl, SiO, GeO, NCl, CaO, SrO, and BaO). These predictions all are presented in Table IV.

Having thus demonstrated the utility of linear quantum capacitance scaling laws, as well as their ubiquity, it is important to ask why or how such fundamental simplicity should prevail amidst the apparent complexity in most other aspects of many-electron quantum mechanics. This question shall be explored in future investigations.

ACKNOWLEDGMENTS

The author gratefully acknowledges valuable conversations with C. Picconatto, S. Das, J. Burnim, A. Gerke, and W. Bunting of the MITRE Nanosystems Group. He thanks J. Klemic and N. Tallapragada of the Nanosystems Group, as well as Professor J. Simons of the University of Utah, for helpful comments on the manuscript. This research was funded by the MITRE Innovation Program and the US Government's NanoEnabled Technology Initiative.

[1] P. J. Lindstrom and W. G. Mallard, eds., *NIST Chemistry WebBook*, NIST Standard Reference Database No. 69 (National Institute of Standards and Technology, Gaithersburg, MD, 2005) [http://webbook.nist.gov/chemistry].
[2] J. Simons, J. Phys. Chem. A **112**, 6401 (2008).
[3] J. C. Ellenbogen, Phys. Rev. A **74**, 034501 (2006).
[4] J. C. Ellenbogen, C. A. Picconatto, and J. S. Burnim, Phys. Rev. A **75**, 042102 (2007).
[5] J. P. Perdew, Phys. Rev. B **37**, 6175 (1988).
[6] G. J. Iafrate, K. Hess, J. B. Krieger, and M. Macucci, Phys. Rev. B **52**, 10737 (1995).
[7] J. C. Maxwell, *A Treatise on Electricity and Magnetism*, Vol. 1 (Clarendon, Oxford, 1873); see especailly pp. 219–221. Available online at [http://posner.library.cmu.edu/Posner/books/book.cgi?call=537_M46T_1873_VOL._1].
[8] G. Woan, *Cambridge Handbook of Physics Formulas* (Cambridge University Press, Cambridge, UK, 2003).
[9] C. Froese, J. Chem. Phys. **45**, 1417 (1966).
[10] C. Froese-Fisher, *The Hartree-Fock Method for Atoms: A Numerical Approach* (Wiley, New York, 1977).
[11] G. Polya and G. Szegö, *Isoperimetric Inequalities in Mathematical Physics*, Annals of Mathematics Studies No. 27 (Princeton University Press, Princeton, NJ, 1951).
[12] T. H. Shumpert and D. J. Galloway, IEEE Trans. Antennas Propagation **25**, 284 (1977).
[13] C. F. Bunge and J. A. Barrientos, At. Data Nucl. Data Tables **53**, 113 (1992). Data from this paper are available online at [http://server.ccl.net/cca/data/atomic-RHF-wavefunctions/tables].
[14] C. A. Picconatto, unpublished density functional theory calculation at The MITRE Corporation to determine the electron affinity of H_2.
[15] L. Hanley, J. L. Whitten, and S. Anderson, J. Phys. Chem. **94**, 2218 (1990).
[16] F. A. Gianturco and F. Schneider, J. Phys. B **29**, 1175 (1996).
[17] The author thanks Mr. W. Bunting of the MITRE Nanosystems Group for pointing out the anomalous scaling behavior of some heavy atoms.
[18] J. R. Sabin, S. B. Trickey, S. P. Apell, and J. Oddershede, Int. J. Quantum Chem. **77**, 358 (2000).
[19] A. I. Boldyrev, J. A. Simons, and D. A. Boldyrev, *Diatomix Database: Experimental and Ab Initio Molecular Constants of Diatomic Molecules* (Wiley, London, 1997), plus references cited therein.
[20] G. Gutsev, M. Nooijen, and R. Bartlett, Chem. Phys. Lett. **276**, 13 (1997).
[21] J. C. Rienstra-Kiracofe, G. S. Tschumper, H. F. Schaefer III, S. Nandi, and G. B. Ellison, Chem. Rev. **102**, 231 (2002), plus references cited therein.
[22] S. Smoes and J. Drowart, J. Phys. Chem. **95**, 5435 (1991).
[23] I. Shim, K. Mandix, and K. Gingerich, J. Chem. Soc., Faraday Trans. 2 **80**, 1171 (1984).
[24] H. Partridge, J. C. W. Bauschlicher, and P. Siegbahn, Chem. Phys. Lett. **97**, 198 (1983).
[25] H. W. Sarkas, S. T. Arnold, J. H. Hendricks, V. L. Slager, and K. H. Bowen, Z. Phys. D **29**, 209 (1994).
[26] C. J. Reid, Chem. Phys. Lett. **229**, 279 (1994).
[27] F. Grein and A. Kapur, J. Mol. Spectrosc. **99**, 25 (1983).
[28] N. Brinkmann, G. Tschumper, and H. F. Schaefer III, J. Chem. Phys. **110**, 6240 (1999).
[29] D. R. Lide, ed., *Handbook of Chemistry and Physics*, 89th ed. (CRC, Boca Raton, FL, 2008). See especially tables of atomic IPs on pp. 10–203 to 10–205 and EAs on pp. 10–156 to 10–157.
[30] H. Ebinghaus, Z. Naturforsch. A **19**, 727 (1964).